Amplification of stick-slip events through lubricated contacts in consolidated granular media

Belfor Galaz,[1] David Espíndola,[2] and Francisco Melo[1]

[1]*Departamento de Física, Universidad de Santiago de Chile, Av. Ecuador 3493, Casilla 307, Correo 2, Santiago, Chile*

[2]*Joint Department of Biomedical Engineering, University of North Carolina at Chapel Hill and North Carolina State University, 109 Mason Farm Road, CB 7575, Chapel Hill, North Carolina 27514, USA*

(Received 29 May 2018; published 24 October 2018)

The influence of lubricated contacts on the stick-slip behavior of a granular system is investigated. Samples of cylindrical shape made of glass spheres confined at a constant pressure and subjected to gradual deformation along their main axis are considered. Under constant axial deformation, the granular compact exhibits a regular stick-slip regime, in which gradual stress loading (stick) is followed by rapid relaxation events or failure (slip). The amplitude of stress drops (slips) and their recurrence time are investigated as a function of the amount of lubricant fluid. In the absence of lubricant, stress drops are very frequent but their amplitude is relatively small. However, the addition of a minute volume of lubricant into the granular packing, increases both the amplitude of stress drops and their recurrence time, following a saturating exponential loading curve with the lubricant volume. We show that the typical volume at which saturation occurs corresponds to the amount of fluid required to completely cover the surface of the spheres, with the thickness of the coat corresponding to the size of the asperities. These results support the idea that, to a certain extent, adding lubricant reduces sliding friction, as well as synchronously mobilizes a set of contacts.

DOI: 10.1103/PhysRevE.98.042907

I. INTRODUCTION

Stick slip, the intermittent sliding motion between solid surfaces in contact, is a common frictional phenomena expressed over distinct spatial scales, ranging from atomic [1] to geological scales [2,3]. For instance, elastic energy accumulated during tectonic plate drift is released during the slipping phase, when the tectonic plates yield, in the form of seismic waves or earthquakes [4].

In the context of granular media, frictional phenomenon is important in the study of earthquakes, landslides, and avalanches. Sufficient loading leads to the sudden release of stored elastic or potential energy, potentially leading to catastrophic consequences. The frictional features of the granular layer, created by fragmentation and wear between two tectonic plates, play a pivotal role in the characteristics of earthquakes. Indeed, scaled laboratory experiments have led to an improved understanding of the physical process behind cyclic sliding within a granular fault of geological settles, and its role in the earthquake nucleation and dynamical rupture [5–8].

Often, granular faults contain interstitial fluid that can greatly modify their rheology. However, studying the influence of interstitial fluid on the mechanisms controlling stick-slip events is challenging due to complex laboratory scale experiments, as well as the lack of theoretical models able to explain interactions between grains and effects of pore pressure [9]. The case of a granular fault under conditions of saturated interstitial fluid has been addressed in laboratory experiments; results suggest that fluid-particle interactions may influence the shear stress drop and the recurrence time of stick-slip events, as well as creeplike behavior and strain transients [10–12]. In a sheared quasi-two-dimensional granular system made of elliptical particles, the presence of an interstitial viscous fluid strongly affects the stick-slip behavior and the localization of the deformation [12]. Compared to dry granular conditions, increasing the interstitial fluid viscosity leads to a stronger damping of the stick-slip events as well as a more localized deformation. Recently, further analysis on the effect of fluids on stick-slip behavior has been carried out through three-dimensional (3D) discrete element simulations of dry and fluid-saturated granular fault gouges [13]. Compared to dry conditions, the presence of an incompressible fluid amplifies the drops in shear stress, compaction of granular layer, and kinetic energy release during slip. It was also corroborated that the recurrence time between slip events is longer for fluid-saturated granular fault gouge compared to the dry case.

It is expected that the pore fluid pressure influences the effective normal stress, thus affecting the fault strength. Several mechanisms have been proposed to capture the relation between pore pressure and fault strength during the seismic cycle (see, for instance, [10]). Frictional strength and slip stability on a hydraulically isolated fault is suggested to be controlled by pore pressure fluctuations, resulting from compaction during the interseismic stage of the seismic cycle [14,15]. Conversely, shear induced dilatancy causes pore fluid depressurization and enhances effective normal stress, leading to an apparent hardening. However, to our knowledge, the case of nonsaturated pore has not previously been systematically considered in vanishing added fluid regimes.

This work presents an experimental study of the influence of lubricant on both the amplitude and recurrence time of stick-slip events. Experiments are performed by adding an

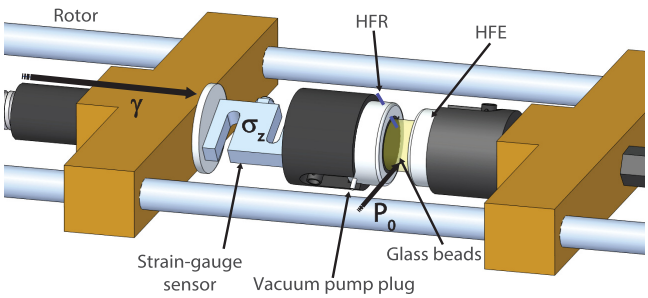

FIG. 1. Experimental setup for a triaxial test on granular samples made of glass beads enclosed in a cylindrical latex membrane. This is closed at both ends by two cylindrical components, containing a flat ultrasonic transmitter (HFE, 25 mm of diameter) and a miniature coda wave receptor (HFR, 2 mm of diameter), which is placed obliquely. Both ultrasonic transducers are hermetically placed inside the cylindrical components ensuring effective pressure confinement. A precision step motor together with a ball bearing screw control axial deformation ($\gamma = vt/L$), whereas a stress gauge and pressure sensors are used to determine total axial stress, $\sigma_z = P_0 + F/A$.

increasing amount of silicon oil to glass beads, ensuring the beads are covered with fluid films with a thickness of the order of asperity size. We use compacted cylindrical samples of granular media confined at controlled pressure [16,17] and subjected to uniaxial compression at a constant strain rate. This type of confinement allows for decoupling of the axial from the radial stress, which is appropriate for modeling the geological fault scenario.

Amplification of the stick-slip behavior is observed, with a sharp increment in the amplitude of the stress drops and their recurrence time. A single slider model, formed of a block-spring system, characterized by two friction coefficients describing the static and the sliding motion, indicates that contact lubrication may considerably reduce kinetic friction, leading to the synchronized mobilization of a glass bead ensemble. These results are consistent with recent numerical studies [18,19].

II. EXPERIMENTAL SETUP

The experimental setup consists of a cylindrical latex membrane hermetically closed by two cylindrical components at each extremity, and filled with glass beads with a mean diameter d; see Fig. 1. Different quantities of lubricant (silicon oil Rhodorsil 47 V 5000), with a cinematic viscosity of 5000 cSt and a dynamic viscosity of 4850 cp at room temperature, are added to the granular packing. This ranges from 0 (dry) to 260 nL/g of glass beads (≈0.043%). A given volume of lubricant and glass beads is vigorously agitated to ensure thorough mixing and that the lubricant is homogeneously distributed. Before pouring the lubricant, glass beads were cleaned by using a Piranha solution, followed by a rinse, first, with abundant distilled water and then with ethanol. Lastly, beads were kept in an oven for one hour to evaporate the residual water and ethanol. This process ensures that the glass beads are free from organic matter and that packing has a minimal humidity. It is important to realize that special care should be taken to fully eliminate residual moisture since it has been reported that the friction coefficient may depend on adsorbed water layers, even after prolongated outgassing [20]. Subsequently, the membrane containing the lubricated beads are placed in a cylindrical acrylic mold of diameter $D = 40$ mm and height L. This mold ensures that both cylindrical components, acting as lids, are parallel to the initial sample shape. The latex membrane assures the lateral expansion of the sample, keeping its volume nearly constant during the axial compression. This was confirmed by measuring the sample mantle through a fringe projection method (data not shown). A constant hydrostatic pressure P_0 is maintained by evacuating the interstitial air through a vacuum pump. Note that P_0 is kept fixed for each experiment but it varies from run to run. This pressure is directly measured by a pressure sensor connected to the vacuum pump. A predetermined quantity of glass beads is set in order to ensure a constant initial packing fraction, $\Phi \approx 0.63$. Once the mold is removed, the sample is mounted in the triaxial test system, where a stepper motor (Parker Compumotor model S106-178MO) is used to apply a constant deformation speed v through a ball bearing screw, which gives the longitudinal strain, $\gamma = vt/L$. The reaction force F produced in response to the imposed deformation, is measured by a strain-gauge sensor, resulting in a stress along the sample axis, $\sigma_z = P_0 + F/A$, where $A = \pi(D/2)^2$ is the sample section. In order to visualize the changes on the structural contact force network, which confirms the stick-slip phenomena, a high frequency emitter ultrasound transducer (HFE) is used to send a two-cycle pulse centered at 320 kHz every 1 s. Under these conditions, acoustic signals of small wavelengths ($\lambda/d \approx 1$) diffuse along different paths of the contact force network. These incoherent transmitted waves, referred to as coda wave signals [see Fig. 3(c)], are very sensitive to contact rearrangements [21] and can be captured by a miniature transducer (HFR) placed to the left side of the sample. The self-demodulated coherent component, described in Ref. [21], is filtered with a high-pass frequency filter with a cutoff frequency of 200 kHz. The global correlation between consecutive coda wave signals is calculated as previously described in [16,17].

III. RESULTS

Prior to investigating the effect of lubrication on stick-slip behavior, we characterized the response of dry glass beads upon compression. First, a triaxial test was performed for incremental levels of confining pressures, ranging from $P_0 = 18$ to 98 kPa [Fig. 2(a)]. Results show that for all confining pressures and for deformations above 5%, the average axial stress σ_z saturates to σ_∞ [Fig. 2(a)]. This saturation confirms that in large deformations, there is relative movement in grain contact and frictional forces are fully mobilized. σ_∞ increases proportionally to hydrostatic pressure P_0 [Fig. 2(b)]. During axial compression we observe a rather homogeneous increase of the sample mantle without the presence of shear banding, indicating that the plastic deformation is not concentrated spatially but rather distributed in the sample, consistent with previous studies [22]. The linear variation of saturation stress value (σ_∞) with the confining pressure (P_0) is then used to estimate the internal friction through the Mohr-Coulomb criterion [23], which gives $\mu_s = 0.33$.

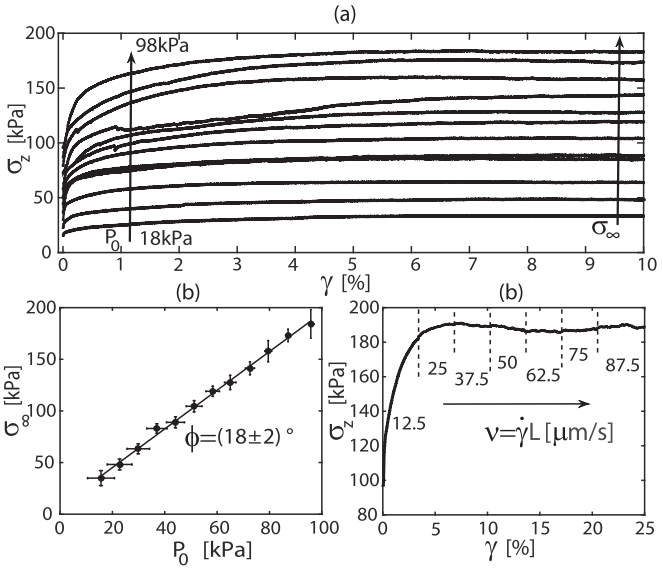

FIG. 2. (a) Stress-strain curves for dry glass beads of $d = 1$ mm and sample length $L = 60$ mm at different levels of hydrostatic pressure, $P_0 = 18$ to 98 kPa, are controlled through the vacuum pump. (b) Saturation stress level σ_∞ as a function of hydrostatic pressure. The continuous line indicates a linear fit, which yields to an internal friction angle $\phi = 18 \pm 2^o$. (c) Strain rate dependency of the stress-strain curve for the case $P_0 = 98$ kPa. The vertical dashed lines limit zones with different deformation speed v, which ranges from 12.5 to 87.5 μm/s.

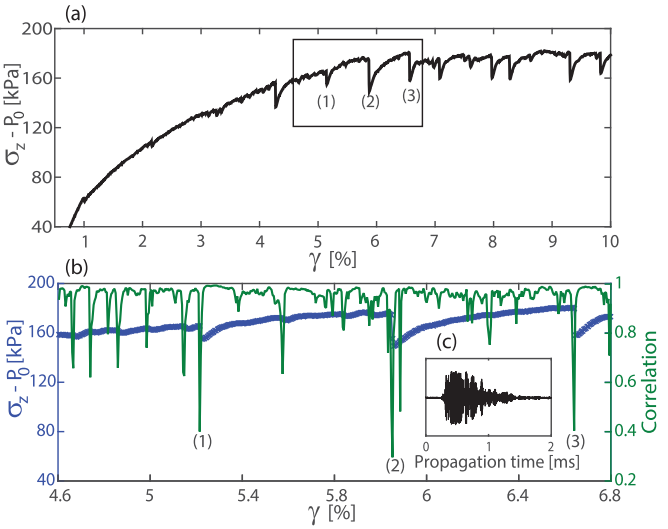

FIG. 3. Stick-slip behavior for the dry contact structural network, visualized using the ultrasonic coda waves correlation coefficient. Experiments performed with glass beads of $d = 2$ mm at a confining pressure of $P_0 = 93$ kPa, in a sample with a length $L = 20$ mm and constant deformation speed $v = 12.5$ μm/s. (a) stress-strain curve showing stress fluctuations and stick-slip events. (b) Overall correlation between consecutive ultrasonic coda wave signals within a selected zone, as in (c) and typical stick-slip events labeled with (1), (2), and (3). (c) Typical coda wave after propagation through the material, detected by the HFR.

In order to evaluate the dependence of axial stress on strain rate, experiments were performed over various deformation speeds v, ranging from 12.5 to 87.5 μm/s, mainly within the saturation regime and for $P_0 = 98$ kPa. These changes of speed were performed *in situ* during the same experiment. The speed was changed with a constant acceleration in such a way that the time of accelerating movement is negligible with respect to the sampling time of the strain-gauge sensor. We observe that under our experimental conditions, the stress-strain curve remains independent of the compression speed [Fig. 2(c)], which is consistent with previous works [24–26]. However, several studies have shown that macroscopic variables, such as sample size, strain rate, and confining pressure, may significantly influence the stick-slip pattern [10,26–29].

We first investigate the stick-slip behavior under dry conditions. The stress strain curve [Fig. 3(a)] shows low fluctuations in stress and stick-slip events, with stress drops of around 20 kPa. Since these events are relatively small, in order to visualize the impact of slip events on the structural network within the granular packing, we used correlation of coda waves propagating through the structural network of contacts. Correlations between two consecutive ultrasonic signals captured with a given delay Δt (corresponding to $\Delta t = \Delta\gamma L/v$) are depicted in Fig. 3(b). Increased decorrelations (down to 0.5) between consecutive ultrasonic signals correspond with the slip events, which are clearly visible through a drop in stress. This is consistent with scenarios where the slip event corresponds to significant structural changes along the entire contact network [16,17,21,30]. These structural changes may be the result of buckling, experienced by the force chains, and sustained by the glass bead contacts, as previously described for creep experiments in similar systems [17].

Figure 4(a) presents the result in the strain-stress curves when lubricant is added during triaxial experiments. It is noted that even a small amount of lubricant generates considerable effects on the stick-slip events. Both a significant increase in the amplitude of the stress drop and the recurrence time are observed, even with a minute volume of lubricant [Fig. 4(a)]. A detailed observation of the stress curves [Fig. 4(b)] reveals that immediately following the stress drop, the local slope remains almost unchanged, indicating that the effective elastic modulus of the material is unaffected by the lubricant. Consistently, the granular compact tends to deform plastically prior to each stress drop, thus triggering an increase in recurrence time. Moreover, a slight hardening is observed with lubricant volume, noted by the increase on yield stress [Figs. 4(a) and 4(b)].

In order to quantify the above effects, the respective averages were measured for stress drop, yield stress, and recurrence time over a sequence of stick-slip events (see Fig. 5). First, the lubricant causes a rapid increase in the amplitude and recurrence time of the stick-slip events, subsequently a saturation occurs for lubricant concentrations above 65 nL/g. It is instructive to express the fluid content as an equivalent thickness of a layer of liquid that would homogeneously cover each particle. Figures 5(a) and 5(b) show that an increase in stress drop and recurrence time reach saturated conditions with a fluid layer thickness within the order of 70 nm. AFM measurements of the surface topography [Fig. 5(c)] reveal that the bead asperity height is dominated by variations lower

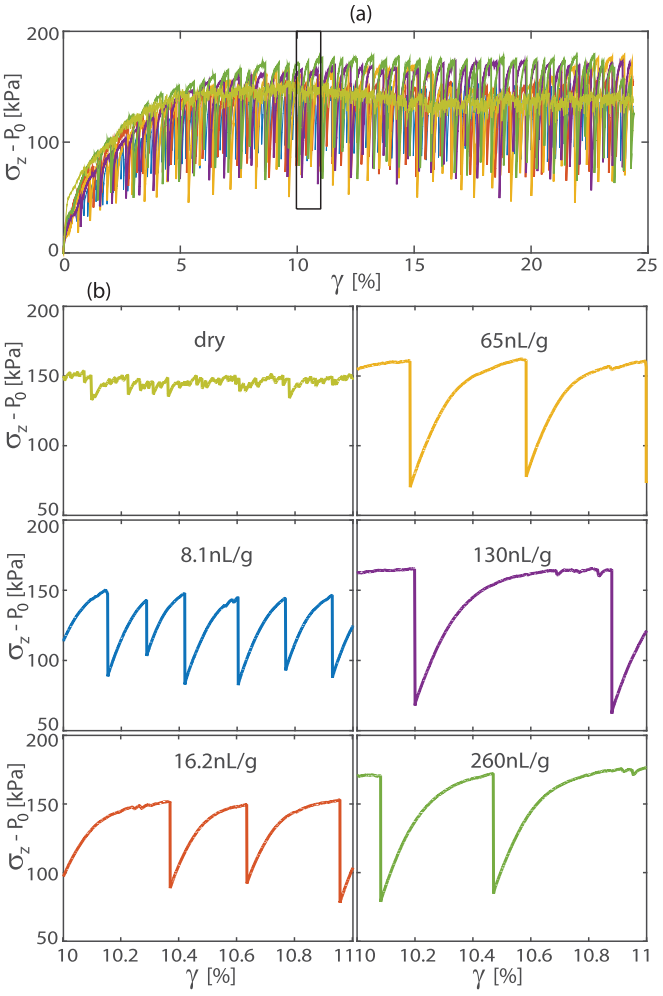

FIG. 4. Stick-slip behavior of lubricated glass bead contacts of $d = 2$ mm at a confining pressure $P_0 = 93$ kPa for a sample length of $L = 60$ mm and constant deformation speed $v = 12.5$ μm/s. (a) Stress-strain curves for different concentrations of lubricating oil, ranging from 0 (dry) to 260 nL/g. (b) Detailed view (zoomed in) of central zone between 10% and 11% strain, showing the amplitude and recurrence time of stick-slip events.

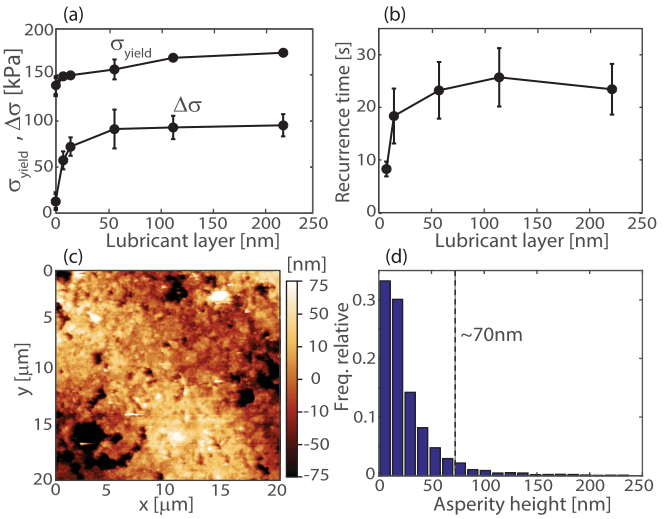

FIG. 5. Stick-slip behavior with slightly lubricated contacts. (a) Amplitude of the stick-slip events $\Delta\sigma$ and yield stress level σ_{yield} as a function of the concentration of lubricant. (b) Recurrence time of stick-slip events. The fluid content is shown in terms of an equivalent lubricant layer thickness considering a homogeneous distribution. (c) AFM image of the asperities of a glass bead. (d) Histogram of the height distribution of the asperities in a glass bead. The dashed line above 70 nm shows the preponderance of height variations below this value.

than approximately 70 nm. The asperity height distribution [Fig. 5(d)] was obtained from AFM images [Fig. 5(c)] by selecting a square area with a side of 20 μm, consistent with the contact area estimated from the lubrication criterion (see discussion section). The dashed line emphasizes the plateau observed in Figs. 5(a) and 5(b) above 70 nm and show the preponderance of height variations below this value in Fig. 5(d). Thus, the highest fluid volumes in this study produce a sufficient lubricant layer to cover the asperities on the bead surface, which confirms that the frictional features are controlled by the lubricant. Despite the addition of a relatively small amount of fluid, the increased slip amplitude, above 50% of the total stress, indicates that the lubricant significantly modifies friction between contacts, leading to an enhanced energy released. Moreover, the increase in yield stress observed in Fig. 4(a), is summarized in Fig. 5(a) leading to relative variation, $\Delta\sigma_{\text{yield}}/\sigma_{\text{yield}}$, that is approximately 13%. This effect is not very significant, but suggests an increment in the static friction coefficient. Indeed, a very recent numerical study demonstrated that at low liquid volumes, cohesive forces between wet particles are responsible for an increase in the coordination number of the packing [19]. This effect leads to more stable particle arrangements, which ultimately enhances frictional strength. Thus, this mechanism may explain strength increase with volumes of liquid, due to an increment in the geometric contribution of the static friction coefficient. Moreover, previous studies have demonstrated that, compared to dry conditions, a small volume of lubricant leads to an increase in the sound speed [31]. This effect was attributed to increased surface contact between lubricated grains, which ultimately increased the contact stiffness [31,32].

IV. DISCUSSION AND CONCLUSIONS

One of the key issues from this study is the structural change occurring within the granular system from strong slip events. Experimental observations indicate that these events are correlated to internal buckling instead of shear banding. Indeed, buckling is directly observed during the triaxial test, as a particle ejected at the surface of the granular packing. This is verified by a characteristic sound emission correlated with an abrupt stress decrease; data not shown.

But why are strong buckling effects not observed in the dry system? In dry samples, buckling events occur but on a significantly smaller scale. The force network is branched, and friction causes fluctuation, i.e., entanglement in the network prevents sliding and large rearrangements, thus limiting the impact from buckling in terms of stress relaxation. By contrast, in lubricated samples, the force network is expected to fluctuate less. This has been corroborated in previous studies

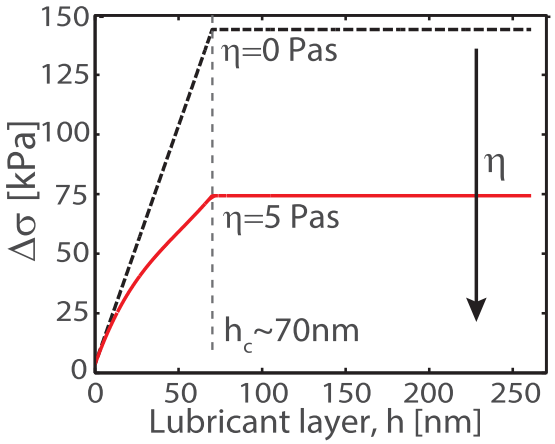

FIG. 6. Stress drop in the function of the lubricant layer for a single slider model with Coulomb's frictional force modified as $f_r \approx (1-\phi_l)\mu_d F + \phi_l \eta\alpha(v/h_c)NS$, with $S \approx 2\pi Rh_c$. (Black dash) Stress drop for the model without viscosity. (Red) Stress drop for a viscosity $\eta \approx 5$ Pas. For this model, the recurrence time is proportional to the stress drop when the sliding time is very small.

using coda wave propagation (see [31] and Fig. 5 in [32]). Indeed, it is shown that the diffusion parameter of coda waves increases with lubricant, due to the increase of the mean free path of these waves, indicating that the force network is less intricate in the presence of lubricant fluid. Therefore, it is expected that in lubricated samples, the force network is dominated by force chains joining each end of the sample. In comparison to dry conditions, these chains hold larger forces. In a less intricate network, the lubricant will enhance contact sliding, ultimately leading to larger stress relaxation events and longer recurrence times.

It is noted that between two slip events within the stress curve, a flat zone (plasticity zone) develops together with the addition of fluid, indicating a significant plastic response in the sample. As observed in Fig. 4(b), this zone grows consistently with fluid content. This is the result of local rearrangement taking place, involving the sliding of a few particles, that only occasionally leads to internal avalanches associated with an abrupt reduction in stress. Thus, the plastic zone of the stress strain curve is due to the continuous occurrence of these small events when the system is close to the yield stress. In the context of the single slider model our results indicate that the lubricant significantly reduces kinetic friction, as well as induces a collective sliding of an ensemble of contacts, maintained together through cohesive forces. As a result of this collective behavior a more stable regime of stick slips, with large recurrence time is produced.

A full understanding of the role of the lubricant on the stick-slip dynamics requires more elaborated frictional models able to connect the physical nature of the contacts with the macroscopic variables. In this context, the shear transformation zone theory, described in [33–35], uses an effective temperature as a measure of the internal disorder and makes this connection. However, applying the shear transformation zone theory to the wet case represents a major challenge because little information is available about the influence of the interstitial fluid on the fundamental variables of this model. We speculate that the incorporation of a small amount of lubricant may slightly increase the effective temperature as a consequence of capillary forces between grains. This increment may reduce the frictional resistance increasing the amplitude of the stick-slip events due to an enhancement on the rate dependence of the frictional force. This mechanism should also explain the stick-slip features for the amount of lubricant above the saturation value [Figs. 5(a) and 5(b)], which requires a detailed modeling of the lubrication at the grains contacts. Therefore, here we adopt a phenomenological point of view based on averaged quantities and we postpone a complete study for a future work.

In order to qualitatively capture the lubrication effect, we consider the simplest frictional Coulomb's model, and we assume that a single lubricated sphere-sphere contact experiences a viscous force that is proportional to the fluid viscosity η and the sliding rate $\dot{\zeta}$, whereas a dry contact experiences a frictional force that is proportional to the applied pressure and the usual friction coefficient. In order to account for the dependence on the amount of fluid added to the sample, we consider the fraction ϕ_l of lubricated contacts. For $\phi_l = 1$, all contacts are fully lubricated. This parameter is related to the volume added per particle as $\phi_l = V/V_c$, where V_c is the volume for which lubrication of the contact is completely achieved with a lubricant layer of thickness h_c and covered surface S.

We notice that for a perfectly smooth pair of spheres, of radius R, separated by a distance h, there exists a finite amount of fluid V_R for which the addition of more lubricant to the contact zone does not significantly affect the shear stress [36]. The latter concentrates at a contact area of radius, $l = \sqrt{2Rh}$ [36]. Thus, $V_R \approx \pi h l^2 = 2\pi h^2 R$. In this context, if N is the number of sphere-sphere contacts in the sample and the lubricant is perfectly distributed over all contacts, lubricant volumes greater than NV_R will not affect shear stress. For the case of rough spheres, under the conditions of fluid-grains mixing employed in our experiments, it is more likely that full lubrication of a contact occurs when films, of thickness close to the upper limit of the height distribution of sphere roughness h_r, totally cover the sphere surface. In this case, we have $V_c \approx 4\pi h_c R^2$, with $h_c \approx h_r$.

With the above assumptions, the average friction force writes $f_r \approx (1-\phi_l)\mu_d F + \phi_l \eta \dot{\zeta} S$, where $S = 2\pi Rh_c$ is the area of the effective lubricated zone between rough spheres and $\dot{\zeta} = \alpha v/h_r$, with v the sliding speed of spheres and α a dimensionless constant.

Solving the motion equation for a single slider of equivalent mass M and stiffness k, the stress drop and the recurrence time can be found. Experimental macroscopic parameters such as the applied force on the sample $F/A = 250$ kPa (A, the sample area), the driven speed $v_0 = 12\,\mu$m, lubricant concentration in terms of the effective thickness of the lubricant layer, and critical lubricant thickness $h_c \approx 70$ nm, are used in this calculation. The effective contact area transforms as $S \to NS$, where N is the number of spheres involved in the sheared zone. The total frictional-viscous force becomes $f_r \approx (1-\phi_l)\mu_d F + 2\pi\phi_l \eta v R\alpha N$, which provides the simplest form accounting for strain rate dependence. The parameter $N\alpha$ is then adjusted to obtain the saturation level of stress drop observed in Fig. 5(a).

We found that a value of the product $N\alpha$ about five times the total number of spheres in the sample allowed one to capture the main experimental features observed in Figs. 5(a) and 5(b). A consistent interpretation of this result is that shear distributes over the whole sample and that the numeric factor $\alpha \approx 5$. This is consistent with the fact that no shear bands were observed in the sample. The factor 5 indicates that probably the fluid layer in the contact zone is slightly smaller than the sphere roughness.

This single model is evaluated for two values of the fluid viscosity (Fig. 6), which shows that both the stress drop and recurrence time increase with the volume of fluid, until a saturation level corresponding to the critical lubricant volume $V = V_c$ is reached. Increasing fluid viscosity reduces this saturation level, capturing the experimental features observed in Figs. 5(a) and 5(b).

In conclusion, this work has carried out a triaxial test on granular media under conditions of pressure confinement. Results show that the incorporation of a small quantity of lubricant induces the formation of a stable regime of stick-slips events, with large amplitude stress drops and recurrence times. This increase becomes saturated when the lubricant concentration is equivalent to liquid layer with thickness greater than the asperity height. The main features of this phenomenon are well captured by recent numerical studies [18,19], where the cohesive forces between wet contacts give a higher coordination number inducing stabilization of the stick-slips events. However, the role of asperity size has not been totally elucidated.

ACKNOWLEDGMENTS

Proyecto Fortalecimiento USA1799-MF072215 and proyecto DICYT 041731GD (Vicerrectoría de Investigación, Desarrollo e Innovación, Universidad de Santiago de Chile) are acknowledged for support. The authors are grateful to L. Caballero for valuable help.

[1] V. L. Popov and J. Gray, ZAMM-Journal of Applied Mathematics and Mechanics/Zeitschrift für Angewandte Mathematik und Mechanik **92**, 683 (2012).
[2] R. Burridge and L. Knopoff, Bull. Seismol. Soc. Am. **57**, 341 (1967).
[3] J. M. Carlson and J. S. Langer, Phys. Rev. Lett. **62**, 2632 (1989).
[4] J. Leeman, D. Saffer, M. Scuderi, and C. Marone, Nat. Commun. **7**, 11104 (2016).
[5] W. Brace and J. Byerlee, Science **153**, 990 (1966).
[6] T. Johnson, F. T. Wu, and C. H. Scholz, Science **179**, 278 (1973).
[7] C. Marone, C. B. Raleigh, and C. Scholz, J. Geophys. Res.: Solid Earth **95**, 7007 (1990).
[8] N. W. Hayman, L. Ducloué, K. L. Foco, and K. E. Daniels, Pure Appl. Geophys. **168**, 2239 (2011).
[9] C. K. C. Lieou, A. E. Elbanna, J. S. Langer, and J. M. Carlson, Phys. Rev. E **92**, 022209 (2015).
[10] M. M. Scuderi, B. M. Carpenter, P. A. Johnson, and C. Marone, J. Geophys. Res.: Solid Earth **120**, 6895 (2015).
[11] M. Blanpied, C. Marone, D. Lockner, J. Byerlee, and D. King, J. Geophys. Res.: Solid Earth **103**, 9691 (1998).
[12] J. E. Reber, N. W. Hayman, and L. L. Lavier, Geophys. Res. Lett. **41**, 3471 (2014).
[13] O. Dorostkar, R. A. Guyer, P. A. Johnson, C. Marone, and J. Carmeliet, J. Geophys. Res.: Solid Earth **122**, 3689 (2017).
[14] R. H. Sibson, Nature (London) **289**, 665 (1981).
[15] N. H. Sleep and M. L. Blanpied, Nature (London) **359**, 687 (1992).
[16] D. Espindola, B. Galaz, and F. Melo, Phys. Rev. Lett. **109**, 158301 (2012).
[17] D. Espindola, B. Galaz, and F. Melo, Phys. Rev. E **94**, 012901 (2016).
[18] O. Dorostkar, P. Johnson, R. Guyer, C. Marone, and J. Carmeliet, in *EGU General Assembly Conference Abstracts*, Vol. 19 (European Geosciences Union, Munich, 2017), p. 3530.
[19] O. Dorostkar, R. A. Guyer, P. A. Johnson, C. Marone, and J. Carmeliet, J. Geophys. Res.: Solid Earth **123**, 2115 (2018).
[20] J. J. Valenza, C.-J. Hsu, and D. L. Johnson, J. Acoust. Soc. Am. **128**, 2768 (2010).
[21] V. Tournat and V. E. Gusev, Phys. Rev. E **80**, 011306 (2009).
[22] M. Oda, Soils Found. **12**, 45 (1972).
[23] R. M. Nedderman, *Statics and Kinematics of Granular Materials* (Cambridge University Press, Cambridge, 2005).
[24] J. Atkinson and P. Bransby, *The Mechanics of Soils: An Introduction to Critical State Soil Mechanics*, McGraw-Hill University Series in Civil Engineering (McGraw-Hill, New York, 1978).
[25] F. Adjémian and P. Evesque, in *EGS General Assembly Conference Abstracts*, Vol. 27 (European Geosciences Union, Munich, 2002).
[26] F. Adjémian and P. Evesque, arXiv:cond-mat/0506547.
[27] E. Aharonov and D. Sparks, J. Geophys. Res.: Solid Earth **109** (2004).
[28] F. Adjemian and P. Evesque, Int. J. Num. Anal. Met. Geomech. **28**, 501 (2004).
[29] K. A. Alshibli and L. E Roussel, Int. J. Num. Anal. Met. Geomech. **30**, 1391 (2006).
[30] Y. Khidas and X. Jia, Phys. Rev. E **85**, 051302 (2012).
[31] T. Brunet, X. Jia, and P. Mills, Phys. Rev. Lett. **101**, 138001 (2008).
[32] S. Griffiths, A. Rescaglio, and F. Melo, Ultrasonics **50**, 139 (2010).
[33] E. G. Daub, *Deformation and Localization in Earthquake Ruptures and Stick-slip Instabilities*, Vol. 70 (University of California, Santa Barbara, 2009).
[34] E. G. Daub and J. M. Carlson, Phys. Rev. E **80**, 066113 (2009).
[35] E. G. Daub and J. M. Carlson, Annu. Rev. Condens. Matter Phys. **1**, 397 (2010).
[36] E. Guyon, J.-P. Hulin, L. Petit, and C. D. Mitescu, in *Physical Hydrodynamics* (Oxford University Press, Oxford, 2015), pp. 277–307.